Molecular Physics
2010, 1–19, iFirst

Taylor & Francis
Taylor & Francis Group

MOLECULAR QUANTUM MECHANICS

A stunning example for a spontaneous reaction with a complex mechanism: the vinylidene–acetylene cycloaddition reaction‡

Elfi Kraka, Hyun Joo† and Dieter Cremer*

Department of Chemistry, Southern Methodist University, 3215 Daniel Ave, Dallas, Texas 75275-0314, USA

(*Received 1 July 2010; final version received 17 August 2010*)

The chelotropic addition reaction (1): singlet vinylidene + acetylene → methylenecyclopropene (MCP), was investigated using different levels of theory (B3LYP, CASSCF, CCSD(T), G2M) and different basis sets (6-31G(d,p), 6-311G(d,p), 6-311++G(3df,3pd), cc-pVTZ). The concerted reaction is spontaneous at room temperature (activation enthalpy of 3 kcal mol^{-1}) and strongly exothermic ($\Delta E = -64$ kcal mol^{-1}; $\Delta H(298) = -59$ kcal mol^{-1}). Analysis of the reaction mechanism with the help of the Unified Reaction Valley approach reveals a complicated sequence of structural and electronic changes, which can be best described by partitioning the mechanism into seven phases: (1) van der Waals, (2) electrophilic attack, (3) biradical, (4) allene, (5) carbene, (6) ring closure, and (7) MCP formation phase. In the transient regions from one phase to the next, structures are located that possess properties of *hidden transition states* (*TSs*) or *hidden intermediates*, i.e. by variation of the electronic nature or the environment of the reaction complex, real TSs and/or real intermediates can be generated. There is indication that a given sequence of reaction phases is fixed for a wide variation in the electronic nature of the reaction complex and that other than just orbital symmetry principles play a decisive role for the reaction mechanism.

Keywords: unified reaction valley approach; vinylidene–acetylene addition; hidden transition state and hidden intermediate; reaction path curvature; reaction phases; reaction mechanism

1. Introduction

There are rules and principles which facilitate the analysis and understanding of the mechanism of chemical reactions. One of the first principles formulated in this connection is the *principle of least motion* (PLM) [1,2], which states that chemical reactions prefer a least motion of the atoms of the reaction complex (RC) combined with a minimum change in the electronic structures of the reactants. Although the PLM can explain numerous low-energy reaction paths (RPs), its shortcomings have also been documented [3–5], especially in connection with the Woodward–Hoffmann rules [6]. There are many examples where non-least motion paths are energetically more favourable than least-motion paths thus suggesting that orbital symmetry represents a more dominant reaction principle than the PLM [7]. The latter tries to combine a nuclear and an electronic part without considering electronic structure in detail [1,2]. Orbital symmetry rules, however, cannot provide reliable predictions with regard to the configuration (stereochemistry) of van der Waals complexes, which are formed early in the entrance channel of chemical reactions and which often play a decisive role for the outcome of a reaction. The configuration of a van der Waals complex between two reactants and by this the best approach mode of the reactants is determined by dispersive, electrostatic, and exchange repulsion effects [8], which can be assessed partly by perturbational MO (PMO) theory [9] and partly by electrostatic considerations in the sense of a multipole interaction analysis.

Reaction rules and principles such as the PLM, the conservation of orbital-symmetry, the aromaticity/anti-aromaticity rules for transition states (TSs) [10], the Hammond postulate, or Polanyi's propensity rules [11] are commonly used in a somewhat ad hoc fashion without clarifying their applicability in a detailed manner. Despite the large amount of evidence collected in the area of reaction mechanism [1–11], many open questions still remain: does the energy provide the best insight into a reaction system to derive

*Corresponding author. Email: dcremer.at.smu.edu
†Current address: University of the Pacific, Stockton, CA, USA.
‡This paper is dedicated to Professor Fritz Schaefer III for his outstanding contributions to Quantum Chemistry.

ISSN 0026–8976 print/ISSN 1362–3028 online

DOI: 10.1080/00268976.2010.519730
http://www.informaworld.com

the reaction mechanism? Or in other words: Are the stationary points on the potential energy surface (PES) most relevant for a mechanistic analysis or, if not, could other PES points be decisive how a reaction proceeds? How can one determine the latter? Can the (non)concertedness of a reaction be predicted? Is there any ranking of rules and principles or does each rule or principle apply exclusively to a typical situation as, e.g. the orbital symmetry rules do?

Apart from these more general questions there are also specific questions such as: Will the configuration of the van der Waals complex formed by the reactants only play a role if it does not contradict orbital symmetry principles? How can one assess the importance of these interactions if a van der Waals complex does not exist? To what extent can the mechanism of a reaction assessed by focusing on the properties of a TS? Is the PLM despite its deficiencies useful to rationalize the reaction mechanism?

For the purpose of clarifying these questions, we have investigated the chelotropic addition of carbene to multiple bonds [12,13], which is normally described by an orbital symmetry principle [6]. A C_{2v}-symmetrical linear approach of a carbene head-on to the midpoint of a CC multiple bond is symmetry-forbidden or, as can also be said on the basis of PMO theory, leads to destabilizing exchange repulsion between the reaction partners. Therefore, the methylene–ethene addition follows a C_s-symmetrical nonlinear path, which is clearly a non-least motion path [12,13]. In this work, we will investigate the chelotropic addition of singlet vinylidene (**V**) to acetylene (**A**) leading to methylenecyclopropene (**MCP**, reaction 1),

$$H_2C{=}C{:}(^1A_1) + H{-}C{\equiv}C{-}H \rightarrow \text{methylenecyclopropene} \qquad \text{(reaction 1)}$$

which in reality follows a C_1- rather than C_s-symmetrical non-least motion path assumed by the orbital-symmetry rules of Woodward and Hoffmann [6]. We will demonstrate for reaction (1) that it is not sufficient just to consider orbital symmetry-rules when predicting the most likely mode of approach between the reactants. One has to understand the different phases of a reaction to make appropriate use of rules based on orbital symmetry, the LMP, or the behaviour of the RC in the van der Waals range. The latter can create a situation in which one of the reaction partners 'dances around' the other (revealed by repetitive rotational and flipping motions) to establish bonding interactions. We also show that despite this non-least motion behaviour of the RC, the PLM can still play an important role in such a reaction.

The far-reaching goal of this work is to learn controlling chemical reactions via a detailed understanding of the reaction mechanism. Understanding of the reaction mechanism implies a powerful tool for its systematic investigation. The tool we apply in this connection is the Unified Reaction Valley approach (URVA) [14–22], which is based on four major assets: (1) the Reaction Path Hamiltonian of Miller *et al*. [23], (2) the IRC of Fukui [24], (3) the generalized adiabatic mode concept of Cremer and co-workers [25–27], and (4) the electron density analysis of Kraka and Cremer [28,29], which is based on Bader's virial partitioning analysis [30]. URVA leads to a detailed analysis of the reaction mechanism providing information on both electronic and dynamic changes of the RC along the RP.

A key element of the URVA investigation is the analysis of the RP curvature. The RP is curved in those regions where major geometric and electronic changes of the RC take place. In previous work, we found that bond breaking and bond forming processes are indicated by a strong curving of the RP [12–22]. Smaller curvature enhancements often indicate a *preparation of the RC* for the actual chemical processes. We also showed that the height of the curvature peaks can be associated with the strength of the bonds being broken/formed, which in turn has consequences for the energetics of a chemical reaction [15–17]. Based on sequence, number, and position of curvature peaks along the RP different reaction phases can be identified and the RP dissected into regions such as the van der Waals regions (positioned in the early entrance and the late exit channel of the reaction), the preparation regions of the RC, and the TS region, in which the chemical processes occur. Using these terms, it has to be emphasized that the existence of a van der Waals complex is not a prerequisite for the identification of a van der Waals region although, if the former exists, it will be located somewhere in the van der Waals region. However, the energy TS does not necessarily relate to the TS region. For example, a TS may be placed in the preparation region [21] because the preparation of the RC for the actual chemical processes leads to an increase of the RC energy whereas the TS region with the chemical processes may be placed far out in the exit channel where the energy is already below the TS energy. An example for such a situation was discussed in the case of the Diels Alder reaction [21].

The mechanistic pattern based on van der Waals, preparation, and TS regions is also found for reactions without a TS as described for the methylene–ethene addition reaction [12,13]. The latter proceeds without a barrier in one strongly exothermic step although four different reaction phases can be distinguished: (1) a van der Waals phase; (2) an electrophilic attack phase

(methylene withdraws density from its reaction partner ethene); (3) a nucleophilic attack phase (methylene donates electron density back to ethene); (4) a ring closure phase. The transition from one reaction phase to the next is indicated by a minimum of the RP curvature, sudden changes in the RP direction, and typical changes in the electronic structure of the RC as reflected by the electron density distribution and the charge populations. At the transition from one phase to another, a hidden TS [13] or a hidden intermediate can be located [20]. We use these terms to express the fact that a change in the electronic nature and/or the environment of the RC can lead to real TSs and real intermediates on the PES, which possess structural and electronic similarities to hidden TS or hidden intermediate [13,20]. We showed, for example, that the barrierless methylene–ethene addition reaction will proceed via a barrier located in the electrophilic attack phase if the methylene is difluoro-substituted where the F atoms make an electrophilic attack of the carbene more difficult thus leading to a raise in energy and a barrier [13].

On the basis of previous results we tentatively suggest that once the mechanism with all its phases has been determined for a prototype of a given reaction, changes in the mechanism can be predicted by considering possible electronic or environmental effects on the RC. In this work, we will verify this hypothesis for reaction (1).

Results of this work will be discussed in four sections. In Section 2, we will shortly describe the computational methods used in this work. In Sections 3, we present the URVA analysis of reaction (1). The chemical relevance of the results of the URVA analysis is discussed in Section 4 with the objective of developing the concepts of hidden TSs and hidden intermediates as a powerful tool for the mechanistic analysis of chemical reactions.

2. Theory and computational methods

Four levels of theory were employed in this work ranging from density functional theory (DFT) [31], to coupled cluster theory including all single and double excitations with a perturbative treatment of the triple excitations (CCSD(T)) [32], GVB-MP2 [33], and G2M [34]. RDFT (restricted DFT) was used for the RP calculations where however in the cases of potential intermediates appropriate tests for internal and external stability of the R solution were carried out [35]. In the case of an external instability, the corresponding unrestricted (U) solution was determined. Singlet open-shell biradicals were treated both with the broken-symmetry (BS) UDFT approach and with the restricted open shell theory for low-spin cases (ROSS-DFT) of Gräfenstein *et al.* [36]. At the ROSS-DFT level, the two-configurational problem is reformulated in a way that one can essentially remain within the realm of single-configuration theory at the cost of building up a more complicated Fock matrix. In summary, DFT calculations were performed at the RDFT, UDFT, BS-UDFT, and ROSS-DFT levels of theory to adequately describe closed-shell molecules and singlet biradicals. The triplet states of the carbenes were investigated to determine the multiplicity of the carbene ground state. In all DFT calculations, the B3LYP hybrid functional [37–39] was applied. DFT calculations of biradicals were checked by CASSCF [40] and GVB-MP2 [33] calculations, where in the former case a (8,8) active space (including the four π MOs and the two singly-occupied σ MOs for biradicals) and in the latter case a (2,2) active space (the two single electrons) were chosen. The GVB-MP2 calculations were performed at the GVB(1) level according to a method developed by Konkoli and Cremer [33] using just the diagonal Fock operator.

Exploratory calculations were performed with the 6-31G(d,p) basis set (basis A) [41]. For the purpose of obtaining more reliable results, all geometry optimizations and frequency calculations were carried out with the 6-311G(d,p) (basis B) and 6-311++G(3df,3pd) basis sets (basis C) [42]. In the case of the CCSD(T) calculations, we employed Dunning's correlation consistent polarized basis set cc-pVTZP (basis D) [43], which is equivalent to a (10s5p2d1f/5s2p1d) [4s3p2d1f/3s2p1d] basis set. All DFT calculations were carried out with the standard pruned (50,194) fine grid [44], which is a reasonable compromise between calculational cost and accuracy.

For each molecule investigated, geometry and vibrational frequencies were calculated at the DFT level utilizing analytical energy derivatives. Vibrational frequencies were used to verify local/global minimum or saddlepoint character of the stationary points found in the geometry optimization, to calculate zero-point energies (ZPE) and entropies at 298 K, $S(298)$, and to obtain absolute enthalpies $H(298)$ and absolute free energies $G(298)$. The latter were utilized to calculate reaction enthalpies $\Delta_R H(298)$, activation enthalpies $\Delta H^a(298)$, reaction free energies $\Delta_R G(298)$, and free activation energies $\Delta G^a(298)$, respectively. Basis set superposition errors (BSSEs) were corrected with the help of the counterpoise method [45]. Charge transfer between the reaction partners was investigated with the help of the natural bond orbital (NBO) [46] and the virial partitioning analysis [30].

The mechanism of reaction (1) was investigated with URVA [14–17]. URVA is based on the fact that

the chemically most important events of a chemical reaction occur along the reaction valley, embedding reactants, transitions state, and products. The $(3K-L)$ dimensional reaction valley (L: number of overall rotations and translations, K: number of atoms of the RC) is spanned by a large amplitude motion defining the RP and the $(3K-L-1)$ vibrational motions orthogonal to the latter. URVA will lead to reliable results if the reaction can be described by one translational mode. In cases where two translational modes are needed a *reaction surface* rather than just a reaction path has to be considered [47]. However, URVA provides still useful qualitative results in this situation [14,15].

The theoretical basis of URVA has been described previously [12–22] and therefore just some essential quantities of the URVA analysis are summarized here. We use the IRC path as RP [48], which is the steepest descent path expressed in mass-weighted coordinates and following the valley floor line. Strictly speaking, this is only true in the convex part of the PES between minimum and the inflection point halfway up to the TS. In the following concave region of the TS, the IRC may deviate from the valley floor line [49]. However, for a mechanistic discussion, small deviations from the floor line are of little concern and therefore we will stick to the IRC path. The RP is given parametrically in terms of its arc length s. The direction of the RP $\tilde{\boldsymbol{x}}(s)$ (tilde denotes mass-weighting) is determined by the RP vector $\boldsymbol{t}(s)$ which is identical to the normalized energy gradient vector $\tilde{\boldsymbol{g}}(\tilde{\boldsymbol{x}}(s))$. The reaction valley is described by $(3K-L-1)$ generalized normal mode vectors $\tilde{\boldsymbol{l}}^g_\mu(s)$ with frequencies $\omega^g_\mu(s)$, generalized normal mode force constants $k^g_\mu(s)$, and generalized normal mode coordinates $Q^g_\mu(s)$ [23].

It is of advantage to express normal vibrational modes in terms of adiabatic internal coordinate modes (AICoMs) [25,27]. An AICoM $\boldsymbol{a}_n(s)$ is a localized, elementary vibrational mode associated with an internal coordinate q_n as for example a bond length, a bond angle, or a dihedral angle [25,27]. AICoMs are based on a dynamic principle (leading parameter principle [5]) and are directly obtained from a modified form of the Euler–Lagrange equations [25]. They are perfectly suited to characterize normal vibrational modes in the common language of chemistry that attempts to express molecular properties in terms of internal coordinates.

The curvature of the RP can be described by the scalar curvature $\kappa(s)$, which is the Euclidian norm of the curvature vector $\boldsymbol{k}(s)$ [14,15,18]. The RP curvature $\kappa(s)$ is related to the sum of the squares of curvature coupling elements $B_{\mu,s}(s)$ describing the coupling between the motion along the RP and the orthogonal vibrational modes spanning the reaction valley [14,15,18]. In this work, we will use adiabatic curvature coupling coefficients $A_{n,s}(s)$ rather than normal mode curvature coupling coefficients $B_{\mu,s}(s)$ to analyse the RP curvature in terms of generalized AICoMs $\boldsymbol{a}^g_n(s)$ of the RC. The graphical representation of the scalar curvature $\kappa(s)$ reveals curvature maxima where energy can flow from one (or more) of the transverse normal vibrational modes into the motion along the RP (or vice versa). The curvature maxima also indicate strong geometric and electronic changes of the RC. In recent work, we have demonstrated that curvature maxima and minima help to partition the RP into different phases representing unique changes in the nature of the RC [15–17].

Kato and Morokuma [50] suggested a procedure to analyse the reaction path vector $\boldsymbol{t}(s)$ in terms of basis vectors $\boldsymbol{u}_n(s)$. Konkoli *et al*. [25] have shown that the vectors $\boldsymbol{u}_n(s)$ represent internal coordinate modes that characterize the movement of the RC along the RP and, therefore, they play a similar role for the translational movement as the adiabatic internal modes do in the analysis of the transverse normal mode vibrations. The weight of the vectors $\boldsymbol{u}_n$ in $\boldsymbol{t}(s)$ is reflected by the amplitudes $A_{n,s}(\boldsymbol{t},s)$ [25].

The RP was first explored at the B3LYP/A level of theory using a constant step size of $0.05\,\mathrm{amu}^{1/2}$ bohr. Then, calculations were repeated at the B3LYP/B level of theory reducing the step size to $0.03\,\mathrm{amu}^{1/2}$ bohr or smaller values (leading to a total of more than 500 path points), which is necessary in connection with the diabatic mode ordering (DMO) procedure of Konkoli *et al*. [19]. DMO resolves all avoided crossings of the vibrational modes along the RP and in this way makes it possible to reliably analyse curvature coupling and mode–mode coupling coefficients. At each path point s, we calculate the RP vector $\boldsymbol{t}(s)$, the internal coordinate modes $\boldsymbol{u}_n$, the forces exerted on the atoms of the RC, the $3K-7$ generalized normal modes $\boldsymbol{l}^g_\mu(s)$ with associated frequencies $\omega^g_\mu(\mathrm{s})$, the decomposition of $\boldsymbol{l}^g_\mu(s)$ in terms of generalized AICoMs $\boldsymbol{a}^g_n(s)$, the adiabatic force constants k^a_n associated with the internal coordinates of the RC, RP curvature $\kappa(\mathrm{s})$, coupling coefficients $B_{\mu,s}(s)$ and $A_{n,s}(s)$, NBO charges, and the electron density distribution $\rho(\boldsymbol{r},s)$. Parts of the analysis were repeated at the CASSCF level of theory [40] employing basis B for the purpose of verifying the DFT description of the reaction mechanism. Only a subset of this data can be presented in this work where calculated properties of the RC generated along the RP are preferentially summarized in diagrams.

URVA calculations were carried out with the program ADIA, which is a multi-purpose package for the analysis of vibrational spectra and carrying out

URVA calculations [18,19,25]. ADIA is a part of the *ab initio* package COLOGNE2010 [51]. For the DFT and *ab initio* calculations, the quantum chemical packages GAMESS [52], GAUSSIAN03 [53], and a local version of CFOUR [54] were used.

3. Mechanism of the chelotropic addition of vinylidene to acetylene

The RP of reaction (1) was explored in the range $s=-3.45$ to $s=10.55\,\mathrm{amu}^{1/2}$ bohr using B3LYP/B. At B3LYP/A, we extended the entrance channel of (1) to $s=-6\,\mathrm{amu}^{1/2}$ bohr, however numerical errors lead to oscillations in the RP direction on a very flat energy plateau being the location of the reactants. Therefore we will preferentially discuss the reaction range investigated with basis B. At $s=-3.45\,\mathrm{amu}^{1/2}$ bohr, the relative energy of the RC (after BSSE corrections of $0.69\,\mathrm{kcal\,mol}^{-1}$) is just $0.06\,\mathrm{kcal\,mol}^{-1}$ higher than that of the separated reactants. Point $s=10.55\,\mathrm{amu}^{1/2}$ bohr corresponds to the position of the product MCP. Results of the URVA analyses are summarized in Figures 1 (change in energy along the RP), 2 (geometric parameters q_n of the RC given as a function of the reaction coordinate s), 3 (decomposition of the gradient in terms of attractive or repulsive internal forces and their change along the RP), 4 (characterization of the RP vector $\boldsymbol{t}(s)$ in terms of internal coordinate modes using amplitudes $A_{n,s}$), 5 (decomposition of the scalar RP curvature κ(s) in terms of adiabatic mode curvature coupling amplitudes $A_{n,s}$(s)), 6 (NBO charge transfer and group charges along the RP), and 7 (geometries of the RC at selected points along the RP).

The addition of $H_2C{=}C{:}(^1A_1)$ to H–C≡C–H yielding **MCP** is strongly exothermic by about $60\,\mathrm{kcal\,mol}^{-1}$ ($\Delta H(298)=-59.2$ (CCSD(T)/D); −59.8 (G2M); $-60.8\,\mathrm{kcal\,mol}^{-1}$ (B3LYP/B, Table 1), which suggests an early TS and a low energy barrier. Calculated energy barriers range from 1.1 to $1.6\,\mathrm{kcal\,mol}^{-1}$ ($\Delta H^{\ddagger}(298)=3.0$ (CCSD(T)/D; G2M/B); $2.9\,\mathrm{kcal\,mol}^{-1}$ (B3LYP/B). Previous investigations of reaction (1) have obtained similar results [55,56]. A linear C_{2v}-symmetrical approach of **V** to **A** is symmetry-forbidden. However, the reaction does not follow a C_s-symmetrical path as found for the addition of methylene to ethene (see [26] and literature cited therein). The RC possesses C_1-symmetry due to a non-linear (sideways) approach of **V** to **A** where the CH_2 group of **V** is rotated out of the plane defined by atoms C1C2C3

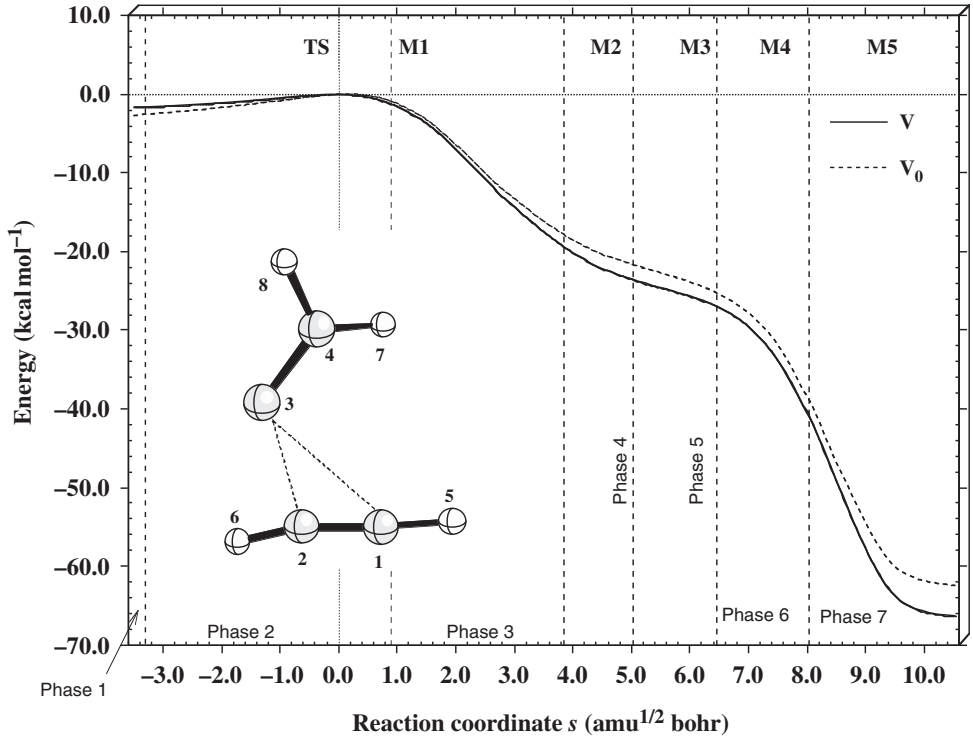

Figure 1. Energy profiles $V(s)$ (solid line) and $V_0(s)$ ($V_0=V+ZPE$) (dashed line) as a function of the RP coordinate s for the reaction $H_2C{=}C{:}$ $(^1A_1)+$ H–C≡C–H → methylenecyclopropene. The position of the TS at $s=0\,\mathrm{amu}^{1/2}$ bohr is indicated by a dotted vertical line. The RC and the numbering of atoms used in this work is also shown. Different phases (phases 1 to 7) of the reaction mechanism are indicated by the positions of the curvature minima M1 to M5 (dashed vertical lines). B3LYP/6-311G(d,p) calculations.

Table 1. Energies ($E, \Delta E$), enthalpies ($\Delta H(298)$), and free energies ($\Delta G(298)$) for reactions (1) and (3) calculated with different methods.[a]

	ΔE			$\Delta H(298)$			$\Delta G(298)$		
Method	Reactants	TS[b]	Product	Reactants	TS	Product	Reactants	TS	Product
Reaction (1)									
B3LYP/A	−154.59291	0.9	−72.4	−154.53436	2.0	−67.80	−154.58245	10.7	−56.4
B3LYP/B	−154.63999	2.0	−65.4	−154.58148	3.2	−61.0	−154.62945	12.1	−49.7
B3LYP/C	−154.65570	1.6	−65.2	−154.59718	2.8	−60.8	−154.64513	11.7	−49.5
CCSD(T)/D	−154.30401	1.7	−63.7	−154.24549	3.0	−59.2	−154.29344	11.9	−47.9
G2M	−154.36066	1.8	−64.1	−154.30214	3.0	−59.8	−154.35015	11.9	−48.5
Reaction (3)	(a) X = F								
B3LYP/B	−353.12683	–	−84.0	−353.07940	–	−81.2	−353.13208	–	−70.0
	(b) X = Cl								
B3LYP/B	−1073.85767	–	−77.7	−1073.81264	–	−74.7	−1073.86856	–	−63.0
	(c) X = Br								
B3LYP/B	−5301.70958	0.0	−72.8	−5301.66519	0.4	−69.9	−5301.72511	9.8	−57.4
	(d) X = I								
B3LYP/B + SDD	−176.25095	3.1	−67.2	−176.20694	3.5	−64.3	−176.26868	13.3	−51.9

Notes: [a]Absolute energies in Hartree, energy differences ΔE and enthalpy differences ΔH in kcal mol^{-1}. For CCSD(T) vibrational and thermal corrections were taken from DFT/C results. Relative energies (enthalpies) of TS and product are given with respect to the reactants. Basis A: 6-31G(d,p); B: 6-311G(d,p); C: 6-311++G(3df,3pd); D: cc-pVTZ; SDD: Stuttgart–Dresden effective core potentials [57].
[b]BSSE corrected values.

(Figures 1 and 7). In this way, exchange repulsion between the in-plane lone-pair electrons at the carbene atom C3 and the π-system of **A** is largely reduced whereas on the other side the empty pπ orbital at C3 can still overlap with the occupied in-plane π-orbital of **A** (see below).

The energy profile of the reaction (Figure 1) confirms the existence of a small barrier located far out in the entrance channel and a steep descent toward the minimum occupied by **MCP**. However, Figure 1 reveals also a peculiarity of the energy profile along the RP: there is a broad shoulder of the energy function in the range from $s = 4$ to $7\,\text{amu}^{1/2}\,\text{bohr}$, which is confirmed when carrying out CASSCF calculations. The shoulder suggests the existence of (a) hidden intermediate structure(s) in the range $s = 4$ to $7\,\text{amu}^{1/2}\,\text{bohr}$ that is (are) not stable enough to occupy a local minimum on the PES, however which is (are) important for a detailed understanding of the reaction mechanism. There is also indication for the existence of intermediate structures when inspecting Figure 2 (geometric changes of RC: several internal coordinates of the RC adopt minimal or maximal values in the range of the energy shoulder) and Figure 3 (changes in the RP direction: minimal and maximal values of internal coordinate contributions to path direction). In line with these observations is the fact that the changes in the internal forces of the RC along the RP (Figure 4) reveal that close to $s = 5\,\text{amu}^{1/2}\,\text{bohr}$ the energy gradient is reduced to a value, which is typical of a transient point that is not fully developed as a PES minimum. The gradient must vanish completely at a stationary point such as the TS ($s = 0\,\text{amu}^{1/2}\,\text{bohr}$) or the energy minimum occupied by **MCP** ($s = 10.55\,\text{amu}^{1/2}\,\text{bohr}$; not shown in Figure 4).

Investigation of the 17 vibrational frequencies spanning the space of the reaction valley orthogonal to the translational motion along the floor of the valley reveals that the RP is unstable between $s = 3.4$ and $s = 5.4\,\text{amu}^{1/2}\,\text{bohr}$ because the lowest vibrational frequency of the RC becomes imaginary. This is the range of the shoulder in the energy profile (Figure 1) and indicates that the RP follows a small energy ridge on a flat, inclined part of the PES. We note that the choice of the coordinates may have an impact on the frequencies of vibrations orthogonal to the RP [15,58,59]. A temporary change from real to imaginary and back to real frequencies is normally an indication of a coordinate dependence and may effect in this range curvature couplings. For example, some of the adiabatic curvature coupling coefficients calculated in the range $s = 3.4$ to $s = 5.4\,\text{amu}^{1/2}\,\text{bohr}$ oscillate strongly (small deviations from the ridge path lead to large changes in the RC geometry). Since we need only qualitative information from curvature couplings, the mechanistic analysis can be carried out nevertheless.

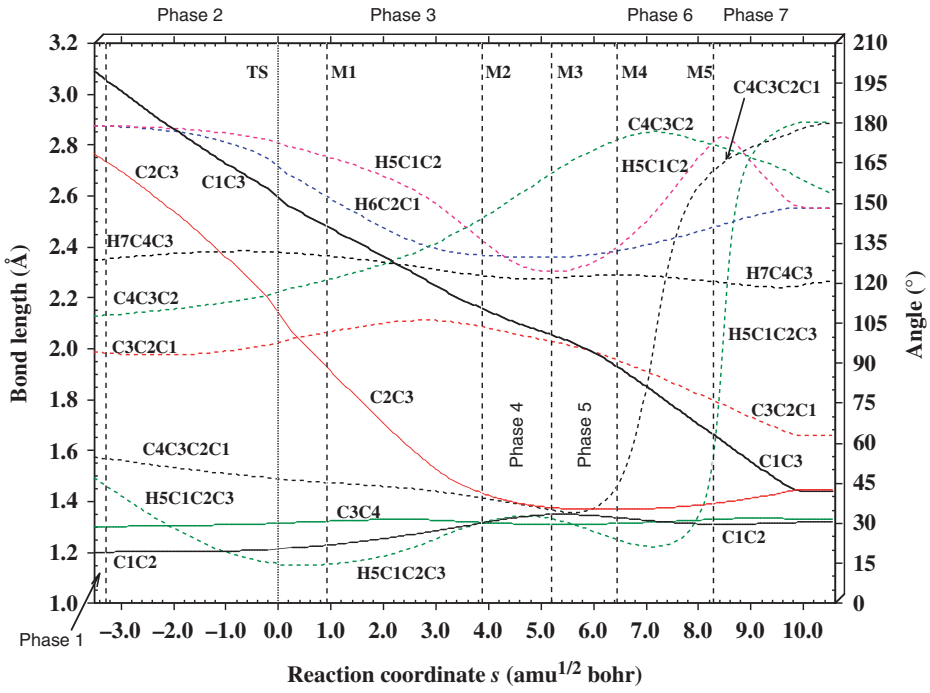

Figure 2. Internal coordinates q_n of the RC given as a function of the reaction parameter s. For a definition of internal coordinates of the RC, compare with Figure 1. The position of the TS at $s = 0\,\text{amu}^{1/2}$ bohr is indicated by a dotted vertical line. The positions of the curvature minima M1 to M5 (see Figure 5) and the phases 1 to 7 are given by dashed vertical lines. B3LYP/6-311G(d,p) calculations.

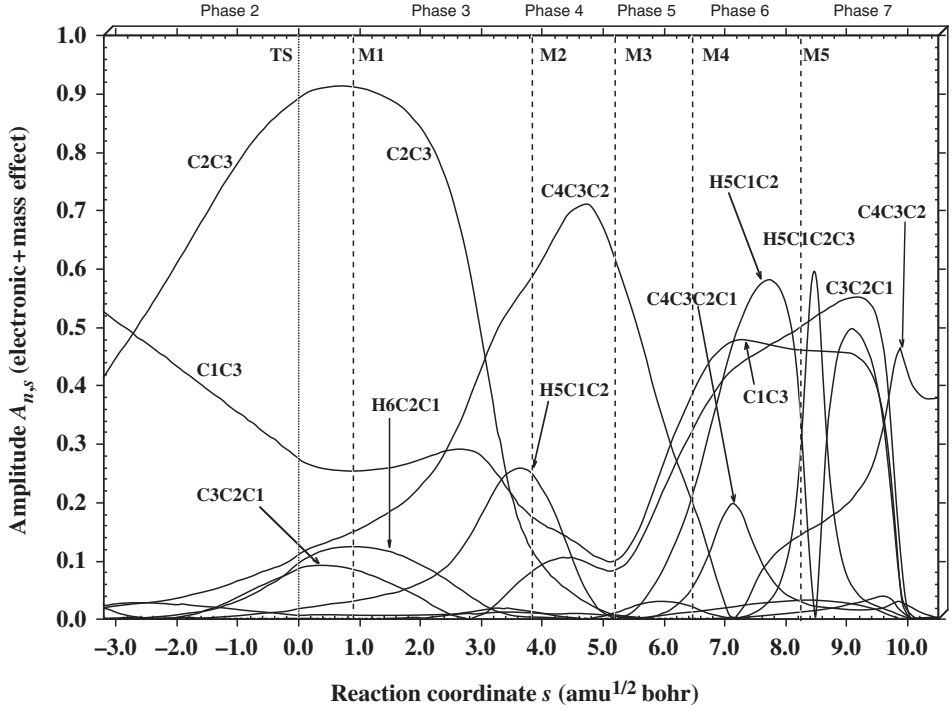

Figure 3. Characterization of the RP vector $\boldsymbol{t}(s)$ in terms of internal coordinate contributions using amplitudes $A_{n,s}$ based on electronic and mass effects. For a definition of internal coordinates of the RC, compare with Figure 1. The positions of the curvature minima M1 to M5 (see Figure 5) and the phases 2 to 7 are given by dashed vertical lines. The position of the TS at $s = 0\,\text{amu}^{1/2}$ bohr is indicated by a dotted vertical line. B3LYP/6-311G(d,p) calculations.

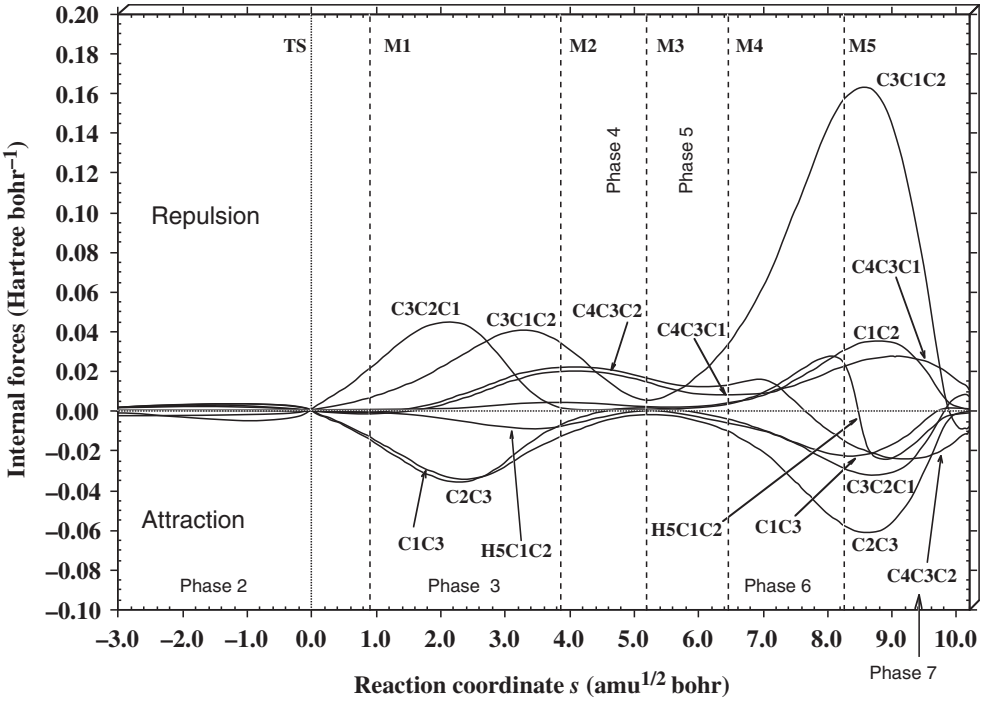

Figure 4. Decomposition of the gradient in terms of attractive or repulsive internal forces. For a definition of the internal coordinates describing the RC, see Figure 1. The position of the TS at $s = 0$ amu$^{1/2}$ bohr is indicated by a dotted vertical line. The positions of the curvature minima M1 to M5 (see Figure 5) and the phases 2 to 7 are given by dashed vertical lines. B3LYP/6-311G(d,p) calculations.

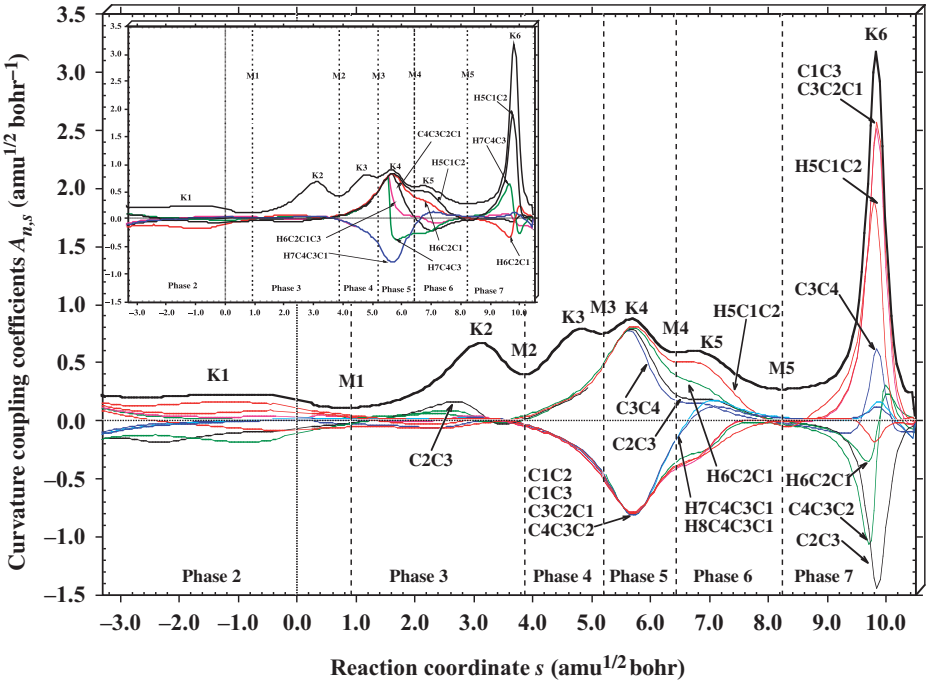

Figure 5. Decomposition of the scalar RP curvature κ(s) (thick solid line) in terms of adiabatic mode-curvature coupling amplitudes $A_{n,s}$(s) (thin lines). A redundant coordinate set was used for the analysis. For a definition of internal coordinates of the RC, compare with Figure 1. The positions of the curvature peaks K1 to K6, curvature minima M1 to M5 are given. Phases 2 to 7 are indicated by dashed vertical lines. The position of the TS at $s = 0$ amu$^{1/2}$ bohr is represented by a dotted vertical line. The insert on the left gives additional adiabatic curvature coupling coefficients not shown in the figure because of readability reasons. For the instability region (3.2 to 5.6 amu$^{1/2}$ bohr), oscillating $A_{n,s}$(s) values have been deleted and only those with a regular behaviour are shown. B3LYP/6-311G(d,p) calculations.

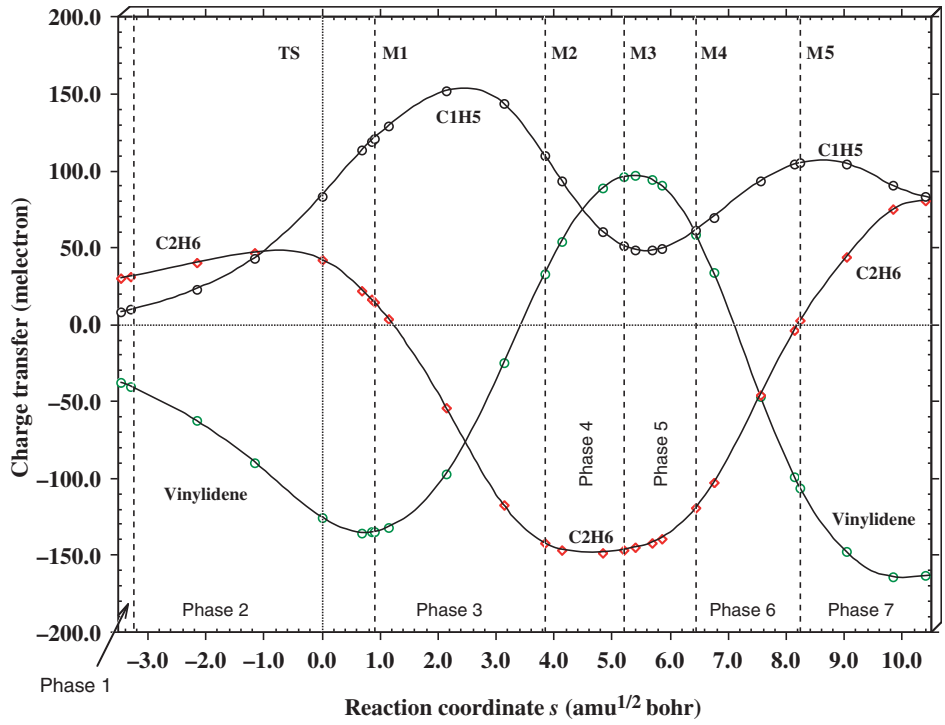

Figure 6. Charge transfer (in melectron) between vinylidene and acetylene according to NBO/B3LYP/6-311G(d,p) calculations given as a function of the RP parameter s. 'Vinylidene' denotes the charge transferred from acetylene to vinylidene (negative sign; positive sign indicates charge transfer from vinylidene to acetylene), 'C1H5' is the group charge of the C1H5 group, and 'C2H6' that of the C2H6 group. The positions of the curvature minima M1 to M5 (see Figure 5) and the phases 2 to 7 are given by dashed vertical lines. The position of the TS at $s = 0\,\text{amu}^{1/2}\,\text{bohr}$ is indicated by a dotted vertical line. B3LYP/6-311G(d,p) calculations.

A complicated reaction mechanism is suggested by the RP direction and the RP curvature diagrams of Figures 3 and 5. Five different internal coordinates (C1C3, C2C3, C4C3C2, H5C1C2, H5C1C2C3) dominate the RP direction at different stages of the reaction, however in each case with substantial contributions from six or seven other internal coordinates. Symmetry-allowed reactions are usually characterized by a collective change of many internal coordinates of the RC, however in all cases studied so far [13,14,21,22] these changes are all relatively small where in the present cases relatively large changes in the internal coordinate contributions to the RP direction can be found throughout the whole reaction (Figure 3). The impression of a rather complex reaction mechanism is confirmed when inspecting the curvature diagram. A total of five smaller curvature peaks (K1 to K5) and one larger curvature peak K6 can be observed (Figure 5). Each of these curvature peaks represents an important structural change of the RC [13,16] and therefore we base the mechanistic analysis of the reaction on the curvature diagram.

We dissect RP (1) in different phases where a phase is defined as the RP region spanning from one curvature minimum to the next. Considering the fact that before $s = -3.30\,\text{amu}^{1/2}\,\text{bohr}$ only weak van der Waals interactions lead to changes in the geometry of the RC (the curvature is close to zero in the range $s = -5.5$ to $-3.3\,\text{amu}^{1/2}\,\text{bohr}$ as investigated at B3LYP/A), it is useful to call reaction phase 1 a van der Waals region. In this way, seven different mechanistic phases can be distinguished for reaction (1). In the following we will discuss the mechanistic phases one by one.

- **Phase 1: van der Waals range from $s = -5.50$ to $-3.30\,\text{amu}^{1/2}\,\text{bohr}$.** Molecule $H_2C{=}C{:}(^1A_1)$ possesses a dipole moment of 2.5 Debye (B3LYP/B) and therefore it can polarize the density of **A** when approaching the latter sideways with C4 rotated out of the C1C2C3 plane by 54° (see Scheme 1). In addition, the CH_2 group is rotated by 13.5° at the C4C3 bond to reduce destabilizing exchange interactions between the CH bonds and

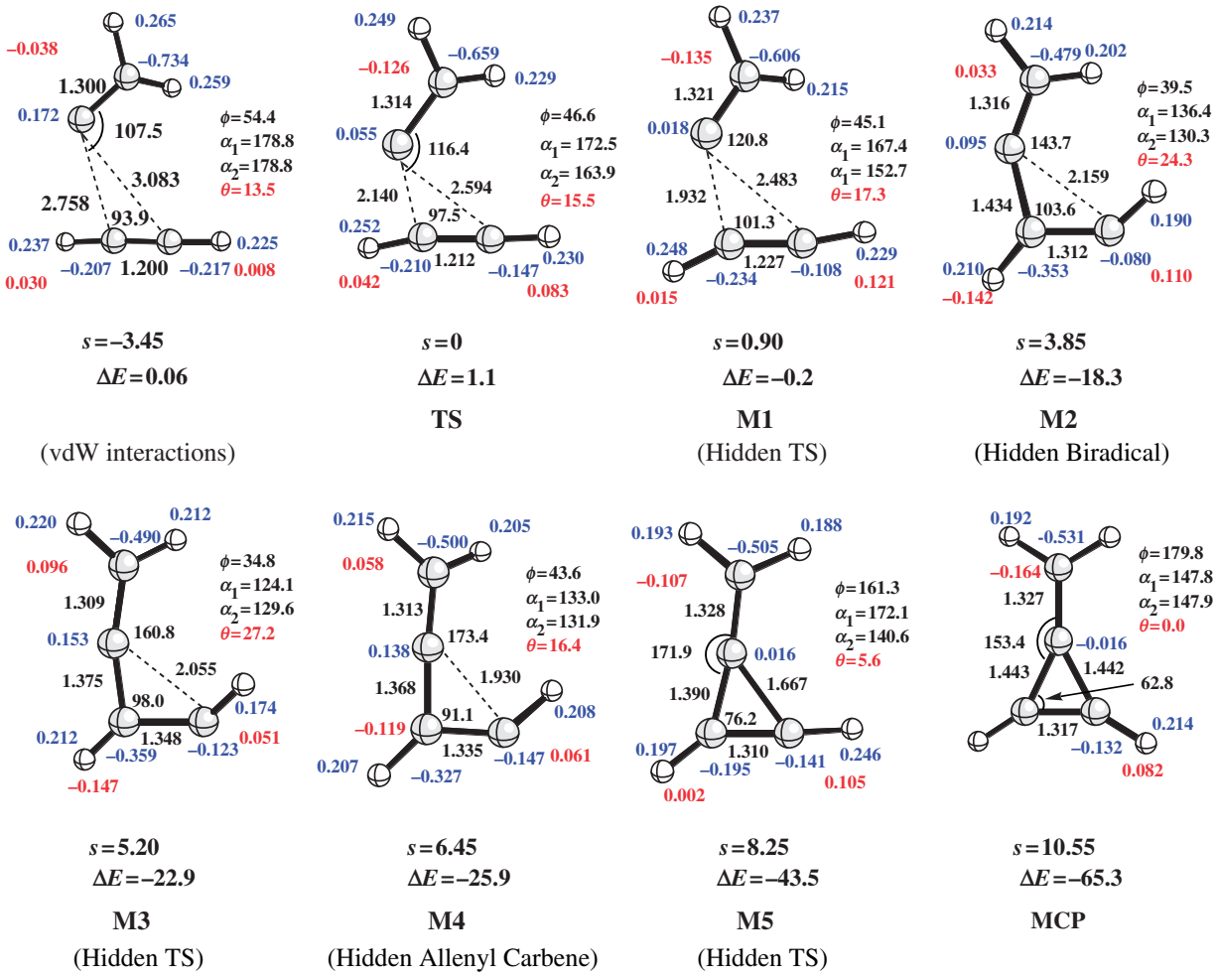

Figure 7. Geometry and NBO charges of the RC at distinctive points s along the RP defined by the minima of the curvature diagram of Figure 5. The NBO charges are given for each atom in small blue print and the resulting group charges determining the charge transfer in red print. The dihedral angle C1C2C3C4 is given by ϕ; α_1 and α_2 give the H5C1C2 and H6C2C1 bending angle, and θ is the rotation angle of the CH_2 group. Bond lengths in Å, angles in degree, NBO charges in electron. B3LYP/6-311G(d,p) calculations.

between the π-electron systems of the reactants. At the beginning of the van der Waals range ($s=-5.50\,\mathrm{amu}^{1/2}\,\mathrm{bohr}$; B3LYP/A calculations) there is just a moderate charge transfer of one melectron from **A** to **V** accompanied by negligible distortions in the geometry of the reactants (as done previously [13] we define the start of the van der Waals range to correspond to that s-point at which 1 melectron is transferred). At $s=-3.30\,\mathrm{amu}^{1/2}\,\mathrm{bohr}$, the charge transfer has increased to 40 melectron and the energy of the RC is $0.1\,\mathrm{kcal\,mol}^{-1}$ higher than that of the separated reactants, with little changes in the bond lengths and bond angles (Figure 7) (the end of the van der Waals region is set, somewhat arbitrarily, to an increase of $0.1\,\mathrm{kcal\,mol}^{-1}$ in the energy of the RC [13]). The RP direction is dominated by coordinates C1C3 and C2C3 (Figure 3; compare also with Figure 1 for numbering of atoms), which are the approach parameters of the two reactants. There are just negligible internal forces distorting the RC (Figure 4).

Although the changes in energy, geometry or electronic structure in the van der Waals phase are minimal, the dipole-induced dipole interactions between the reactants (Scheme 1) are decisive for the stereochemistry of the RC. For example, the geometry of the RC avoids destabilizing interactions, however provides at the same time a stabilizing charge transfer from **A** to **V**, which is typical for all chelotropic carbene addition reactions. [13].

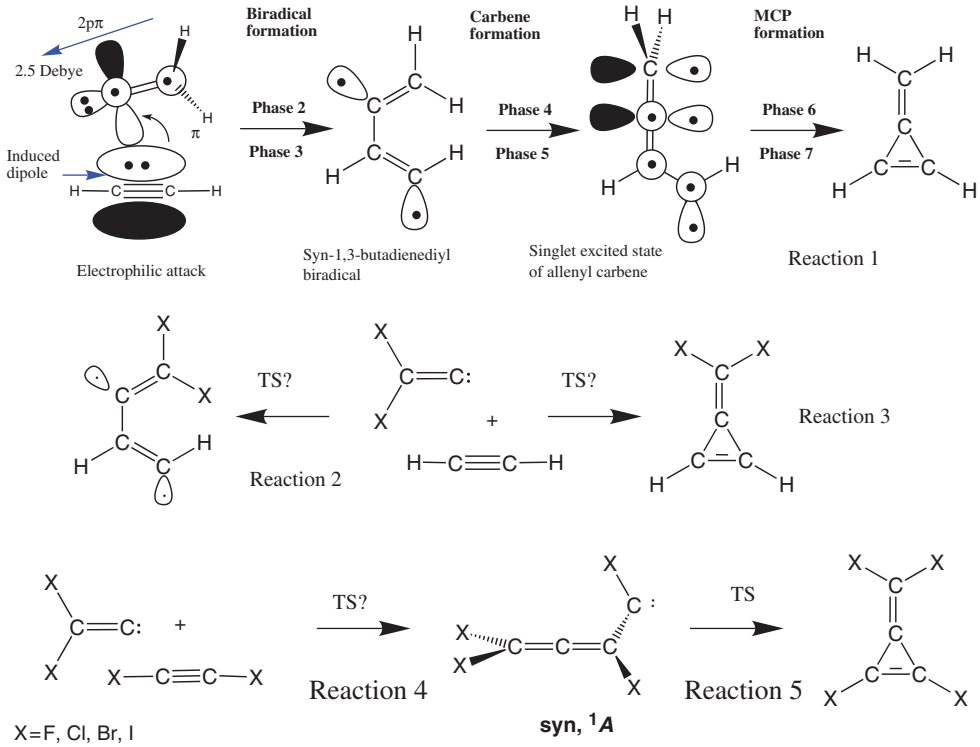

Scheme 1. Schematic representation of reaction (1) in the form of partial reaction steps leading to syn-1,3-butadienediyl biradical and allenyl carbene as potential intermediates. Halogenated reaction partners can lead to syn-1,3-butadienediyl biradical (reaction 2), methylenecyclopropene (reaction 3), syn-allenylcarbene (reaction 4) or from allenylcarbene to methylenecyclopropene (reaction 5).

Despite of the non-optimal approach of **V**, there is sufficient overlap between the empty pπ orbital at C3 and the π-system of **A** to transfer negative charge from the donor **A** to the acceptor **V** in the sense of an electrophilic attack (Scheme 1, reaction 1). By this the actual chemical processes of reaction (1) are initiated.

- **Phase 2: electrophilic attack range from $s = -3.30$ to 0.90 amu$^{1/2}$ bohr.** The first curvature enhancement K1 is located in this region thus indicating that there is a change in the geometry of the RC (Figure 5). Both CC bonds are lengthened due to the charge transfer which increases toward the end of the electrophilic attack range to 135 melectrons (Figure 6). For **A**, depopulation of the two π MOs accompanied by a polarization of the density from C1 to C2 leads to some double bond character and a *trans* arrangement of the CH bonds, whereas the charge transferred to **V** populates antibonding C3C4 MOs thus weakening this bond.

In the case of the methylene–ethene addition [13], the pπ orbital of methylene is completely empty and the reaction proceeds without an energy barrier once the RC has been formed via electrostatic attraction. As soon as the pπ orbital of the carbene is partly occupied because of π-electron donating substituents as in :$CF_2(^1A_1)$, charge transfer from ethene to carbene becomes more difficult and accordingly a barrier is generated in the electrophilic attack phase [13]. Although **A** and ethene differ with regard to their π-donating ability thus excluding a direct comparison of the carbene–ethene and carbene–acetylene reaction, we observe an important similarity to the carbene–ethene addition when analysing the **V**–**A** reaction: Because of interactions between the empty pπ and the pseudo-π-orbital of the CH_2 group of **V**, the former obtains an electron population of 114 melectrons, which makes charge transfer to this orbital more difficult. This leads to the formation of a small energy barrier somewhat after the location of curvature enhancement K1 where the

structural changes in phase 2 take place (Figure 5).

As in the case of other symmetry-allowed reactions, changes in the electrophilic attack phase are relatively small, involve many internal coordinates with small distortions, and stretch over four s-units of the RP. At the end of this process structure M1 is obtained that resembles the TS structure: the TS of C2C3 bond formation is obtained with a maximum (−135 melectrons, Figure 6) of charge transferred to V, a *trans*-distortion of **A**, and a bending away of the CH_2 group of **V** to avoid steric repulsion.

- **Phase 3: Biradical formation range from $s = 0.90$ to $3.85\,\text{amu}^{1/2}$ bohr.** In a carbene–ethene reaction, the electrophilic attack range is followed by the nucleophilic attack range [26]. In this phase, charge transfer is reverted, the alkene becomes the acceptor and the carbene via its electron lone-pair the donor. The charge transfer is accompanied by rehybridization at the carbene C atom and a reorganization of charge. The same observations can be made for the **V**–**A** reaction as observed in phase 3 of the charge transfer diagram (Figure 6). The bond formation C2C3 is finished in this phase as reflected by the fact that the adiabatic curvature coupling coefficient C2C3 significantly contributes to curvature peak K2 (Figure 5) and that there is an attractive internal force C2C3 in the internal force diagram (Figure 4). The RP direction is dominated by coordinate C2C3 both in phases 2 and 3 (Figure 3), which is indicative of the formation of this bond.

  The curvature minimum M2 indicates the formation of a transient structure, which is not stable enough to occupy a local minimum on the PES. Nevertheless, M2 is relevant for the reaction mechanism. Inspection of structure M2 in Figure 7 suggests the formation of a distorted, 40°-rotated, *cis*-1,3-butadienediyl biradical. There are radical centres at C1 and C3 as a result of the C2C3 bond formation. The C-framework is characterized by two short CC bonds (1.316 and 1.312 Å, Figure 7) and a longer central bond (1.434 Å) reminding of the butadiene CC-bonding pattern. Structure M2 is located where the shoulder in the energy profile of reaction (1) develops. Tentatively, we call M2 a hidden intermediate that may arrange to a real intermediate when electronic and environmental conditions of the reaction support this.
- **Phase 4: Linearization range from $s = 3.85$ to $5.20\,\text{amu}^{1/2}$ bohr.** In this phase, curvature minimum M3 is reached after passing curvature enhancement K3. M3 is exceptional in so far as it has an almost linear C2C3C4 unit with a significantly shortened C2C3 bond (1.375 Å, Figure 7). Almost 100 melectrons are transferred from the **V** to the **A** unit thus increasing the polarization of the latter into a more positive C1H5 and a more negative C2H6 end (Figure 6). Angle C2C3C4, which quantifies the linearity of the C2C3C4 unit, dominates the direction of the RP (Figure 3). Since (a) M3 is positioned in an unstable path range and (b) the curvature minimum M3 is rather flat (Figure 5), we refrain at this point from any further investigation of phase 4 and M3.
- **Phase 5: Carbene formation range from $s = 5.20$ to $6.45\,\text{amu}^{1/2}$ bohr.** Curvature peak K4 dominates phase 5 and is caused by a repositioning of the CH_2 group, bonds C1H5 and C2H6 as well as changes in the bonds C1C3 and C1C2 as reflected by the adiabatic curvature coupling coefficients (Figure 5). The RP direction is dominated by the linearization parameter C4C3C2 and distance C1C3. Structure M4 generated at the end of phase 5 resembles a distorted syn-allenyl carbene in its singlet excited state (Figure 7, Scheme 1). Our assignment is based on the linearity of the C4C3C2 unit, the rotation of the CH_2 group by 16 up to 27° (relative to the plane C1C2C3). Allenyl carbene itself would have a planar C-framework (rather than a C4C3C2C1 angle of 44°), a CH_2 group perpendicular to the plane C1C2C3, and its lowest singlet state would have two electrons in a σ lone pair orbital at C1. M4 instead possesses a delocalized 3-π-system and a single electron in the lone pair orbital at C1 (Scheme 1). Hence, M4 resembles a singlet excited state of allenyl carbene. We assign M4 to a hidden intermediate of allenyl carbene nature. Consequently, M3 should be considered as a hidden TS separating two hidden intermediates M2 (biradical) and M4 (allenyl carbene).
- **Phase 6: Ring closing range from $s = 6.45$ to $8.25\,\text{amu}^{1/2}$ bohr.** Curvature peak K5 (Figure 5) is just a small enhancement after curvature minimum M4. Calculations with different methods and basis sets confirm that

K5 is reproduced independently of the method or basis used. The RP direction is characterized by the flipping of bond C1H5 from a *trans* into a more linear CCH position and the shortening of the C1C3 distance to establish a bond and by this a three-membered ring (angle C3C2C1 is equivalent to distance C1C3 and is shown in Figure 3 just for control purposes). For M5 (Figure 7) a C1C3 distance of 1.667 Å is calculated, which suggests a weak CC bond. Bonding becomes possible because of a rehybridization/reorientation of the two orbitals with the single electrons. The C4C3C2 angle increases from a value smaller than 180° to a value larger than 180° while the CH_2 group adjusts more to the plane of the ring C1C2C3. Also the flipping of the C1H5 bond helps to establish weak bonding interactions between C1 and C3. We describe structure M5 as a hidden TS on the path to **MCP** formation.

- **Phase 7: MCP formation range from $s = 8.25$ to 10.55 amu$^{1/2}$ bohr.** In this phase, the C1C3 bond is finally formed, which is revealed by a large curvature peak K6 dominated by the adiabatic contribution C1C3 (or alternatively angle C3C2C1; Figure 5). In addition, AICoM contributions H5C1C2, H6C2C1, H7C4C3, H8C4C3, and C4C3C2C1 to the curvature peak K6 describe the adjustment to a planar, C_{2v}-symmetrical **MCP** with bonds C1H5 and C2H6 in a *cis*-arrangement. In phases 6 and 7, charge is transferred back from the base of the three-membered ring to the external double bond. This is necessary to convert the **MCP** ring into an aromatic, positively charged (164 melectrons) 2π-system and a polarized slightly negatively charged (−164 melectrons; Figures 6 and 7) external double bond. The dipolar character of **MCP**s (or triafulvenes) is amply known [60] and confirmed by the charge transfer data. The latter makes it possible to estimate the importance of C1C3 bonding. Already in phase 6, exactly at the position of curvature peak K5 ($s = 7$ amu$^{1/2}$ bohr) the switch in charge donation/acceptance occurs (Figures 5 and 6). This means that weak bonding C1C3 interactions are established at a distance of 1.75 Å, which increases to 55% of its final value at M5 according to the charge transfer data. Although these descriptions are just qualitative, they provide further evidence for the characterization of M5 as a hidden TS.

In summary, we can dissect the RP into seven phases, i.e. the location of one real TS, two hidden intermediates M2 and M4 as well as two hidden TSs M3 and M5. This suggests that up to three different chemical reactions can take place, where, because of the electronic conditions of the **V**–**A** system, just one is observed energetically. In the following section, we will discuss the relevance of these observations for the mechanism of carbene reactions and chemistry in general.

4. Chemical relevance of the mechanistic analysis

The concept of hidden TSs and hidden intermediates will only be useful if one can reliably predict under which conditions these transient points on the PES are converted into real TSs and intermediates. In a recent study [55], we systematically scanned the C_4H_4 PES and investigated different forms and states of singlet 1,3-butadienediyl biradicals (**BB**) and allenyl carbenes (**AC**). *cis*-**BB**s such as **1** and **2** (see Scheme 2) were found to be unstable and to directly close to **MCP** whereas *trans*-forms such as **3** and **4** were found to occupy local minima on the PES. Their relative enthalpies are 7–8 kcal mol^{-1} below those of **V** + **A** (Scheme 2) whereas the hidden intermediate M2 is already 18 kcal mol^{-1} (Figure 7) below reactants **V** and **A**. A major reason for the instability of **1** is the low barrier (2 kcal mol^{-1}) for inversion at atom C1. Once **2** is formed, rotation at C2C3 or inversion at C3 lead to **4** (barriers below 5 kcal mol^{-1}), which immediately closes to **MCP**.

4.1. *Enforcing 1,3-butadienediyl biradical*

We investigated various possibilities to stabilize biradical **1** (Scheme 2): (a) introduction of bulky substituents such as tert-butyl groups for H6 and H8 to hinder the formation of **4** by strong steric repulsion. However, the molecule becomes non-planar and closest to **MCP**. (b) Stabilization of the single electrons by three-electron delocalization effects. Radical centres can be stabilized by interaction with a CSi or CCl bond depending on orbital overlap (must be small) and orbital energy differences. In the cases of **6a** and **6b**, stabilization was not sufficient and rearrangement to **MCP** the consequence. (c) We also tried to lock the *cis*-form **1** by establishing a H-bond such as in **7**. This turned out to be not strong enough and the seven-membered ring somewhat strained (Scheme 2) so that again conversion to **MCP** resulted.

However by combining effects (b) and (c) a stable *cis*-butadienediyl biradical can result (**8** in Scheme 3a).

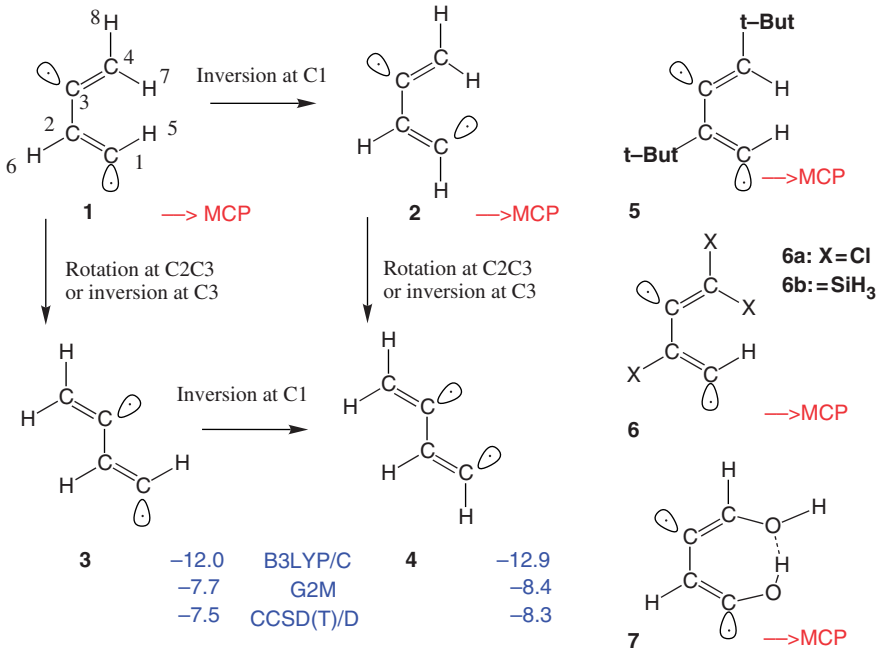

Scheme 2. Interconversion of 1,3-butadienediyl biradicals **1**, **2**, **3**, and **4**. Stabilization of **3** and **4** relative to **V** + **A** given as $\Delta\Delta H_f^0(298)$ values in kcal mol^{-1} as calculated at the B3LYP/C, G2M, and CCSD(T)/D level of theory. Molecules **5**, **6**, and **7** denote potentially stable or metastable 1,3-butadienediyl biradicals. Spontaneous rearrangement to MCP is indicated.

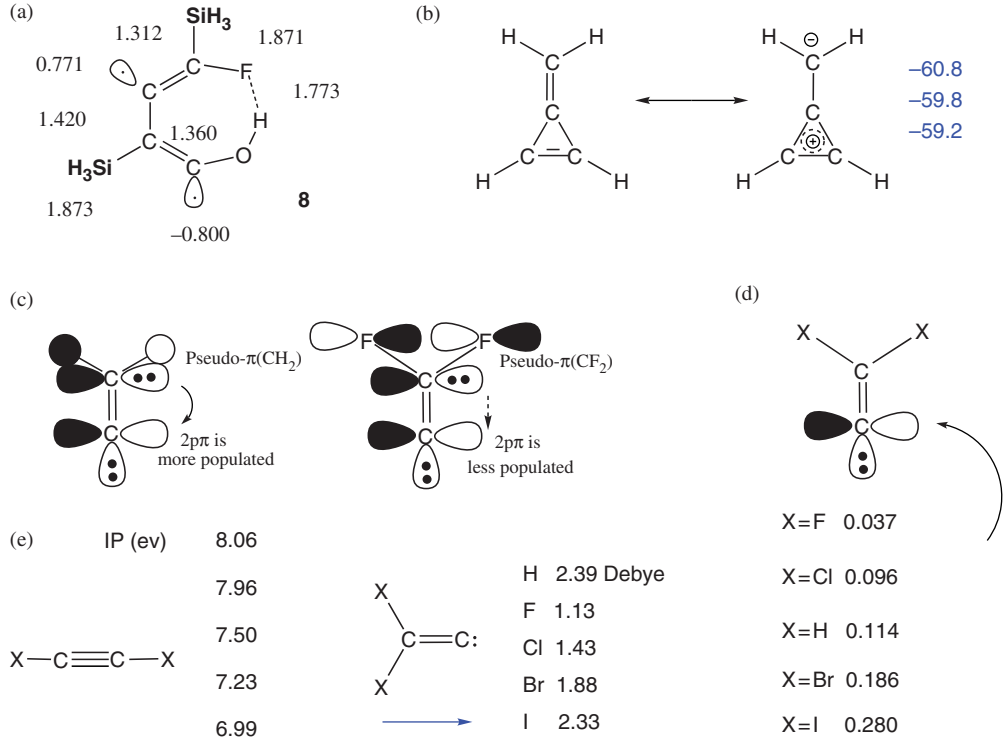

Scheme 3. (a) Stable 1,3-butadienediyl biradicals. (b) Resonance stabilization of **MCP**. Stabilization of **MCP** relative to **V** + **A** is given as $\Delta\Delta H_f^0(298)$ values in kcal mol^{-1} as calculated at the B3LYP/C, G2M, and CCSD(T)/D level of theory. (c) In-plane interactions between the pseudo-π and the π-orbital of **V**. (d) NBO populations of the in-plane pπ orbital. (e) Ionization potentials IP and dipole moments of substituted vinylidenes.

We used the smaller F substituent (thus relieving some strain in the seven-membered ring formed) to establish a tight OH···F H-bond (Scheme 3a). Silyl groups are used to facilitate three-electron delocalization effects without removing too much spin density from centres C1 and C3 so that the electronic nature of a biradical is retained. All vibrational frequencies of **8** are positive thus confirming that the biradical occupies a minimum on the PES.

The above discussion in connection with **8** does not suggest that the biradical is formed via reaction (2) (Scheme 1) where one would have to consider that a 1-silyl-alkyne-2-ol might prefer the corresponding ketene form. Its objective is exclusively to prove the existence of 1,3-butadienediyl biradicals and in general these could be generated via reaction (2) of Scheme 1.

4.2. *Enforcing a barrierless reaction*

As was shown in connection with the methylene–ethene addition reaction, the behaviour of the RC in the electrophilic attack phase can be effectively changed by altering the electrophilicity of the carbene via population/depopulation of the empty pπ-orbital. If this is depopulated relative to the parent compound, the TS in the electrophilic attack phase should vanish and a barrierless reaction results where however the RC passes through the same reaction phases as found for reaction (1). If on the other hand, the pπ-orbital is more populated, the location of the TS should be moved in the direction of the nucleophilic attack phase and the barrier should increase. Population or depopulation of the pπ-orbital depends on the orbital energy of the pseudo-π orbitals of CX_2 (Scheme 3c): when this is lowered with increasing electronegativity of X (relative to X = H), the pπ-orbital is depopulated (reduced donor capacity of CX_2) and prone to accept charge from acetylene. A barrierless reaction should result.

We tested these predictions with the help of reaction (3) (Scheme 1), for which we varied X from F (reaction 3a) to Cl (reaction 3b), Br (reaction 3c), and I (reaction 3d). The population of the pπ-orbital of $X_2C{=}C{:}$ (Scheme 3d) increases from 0.037 and 0.096 for X = F and Cl (both being lower than the reference value of 0.114 electrons) to 0.186 and 0.280 electrons for X = Br and I. For reactions (3a) and (3b), the chelotropic addition proceeds barrierless without a TS directly to the corresponding MCP derivative (see Table 1), whereas all seven reaction phases can still be identified. In the cases of reactions (3c) and (3d) a TS does exist, which is shifted toward the nucleophilic attack phase. However, the calculated barriers (0.01 and 3.1 kcal mol^{-1} after BSSE-corrections; Table 1) are smaller than predicted, which has to do with the fact that $Br_2C{=}C{:}$ and $I_2C{=}C{:}$ possess C_s rather than C_{2v} symmetry because one halogen atom takes a more bridging position. This is a result of the fact that the vinylidene–acetylene rearrangement has increasingly smaller barriers and is shifted more and more to the side of acetylene for the dihalogenated molecules. We note in this connection that we have not investigated scalar relativistic and spin–orbit effects in detail because in this work we are only interested in general trends. However, we included some relativistic corrections by using Stuttgart–Dresden (SDD) effective-core potentials [57].

4.3. *Enforcing an allenyl carbene*

A suitable way of enforcing an allenyl carbene intermediate is to enhance the nucleophilic, electron-donating character of acetylene so that the electrophilic attack of the carbene is made easier. Consequently, back-donation from **V** to **A** and by this the nucleophilic attack become more difficult. This can be realized by halogen-substitution because interactions of the halogen pπ electrons with the acetylene π system leads to an energy rise of the latter (see calculated ionization potentials IP for 1,2-dihalogenoacetylenes in Scheme 3e) and enlarged donor ability. Hence, we investigated the per-halogenated reaction systems (4) shown in Scheme 1.

We expect that there is no longer any TS in the electrophilic attack phase and that the reaction proceeds downhill on the PES until charge back-donation from **V** to **A** and the fact that this is now more difficult leads to the establishment of a new type of energy barrier. The barrier implies the existence of an intermediate, which should possess an allenyl carbene structure. We investigated reaction (4) for X = F (4a), Cl (4b), Br (4c), I (4d) and found our predictions in all four cases confirmed: first an intermediate perhalogenated allenyl carbene is formed, which rearranges via a barrier to the final perhalogenated MCP (reaction 5). The calculated barrier decreases from 17.7 (4a, X = F), 6.9 (4b, Cl), 6.4 (4c, Br), and 5.5 kcal mol^{-1} (4d, I; Table 2), which reflects the fact that the electrophilic attack of **V** is more difficult when varying X from F to I. Accordingly, it becomes increasingly easier to revert charge-transfer between the reaction partners.

Each of the perhalogenated allenyl carbenes should be detectable under matrix isolation conditions provided the corresponding dihalo vinylidene can be synthesized. Sander and co-workers [61] succeeded in synthesizing 1,1-difluorovinylidene and studied the

Table 2. Energies ($E, \Delta E$), enthalpies ($\Delta H(298)$), and free energies ($\Delta G(298)$) for reaction (4) calculated with the B3LYP/6-311G(d,p) level of theory.[a]

Method	ΔE	$\Delta H(298)$	$\Delta G(298)$
	(a) X = F		
Reactants	−551.59882	−551.56350	−551.62165
Allenylcarbene	−82.9	−81.3	−71.4
TS	−65.2	−64.4	−53.8
Methylenecyclopropene	−102.2	−99.7	−88.2
	(b) X = Cl		
Reactants	−1993.07741	−1993.04667	−1993.11089
Allenylcarbene	−51.6	−50.2	−39.4
TS	−44.7	−43.9	−32.1
Methylenecyclopropene	−86.0	−83.5	−71.4
	(c) X = Br		
Reactants	−10448.77736	−10448.74804	−10448.81897
Allenylcarbene	−47.1	−45.7	−34.1
TS	−40.7	−39.7	−27.3
Methylenecyclopropene	−80.6	−78.1	−65.2
	(d) X = I		
Reactants	−197.84821	−197.81984	−197.8951
Allenylcarbene	−45.1	−43.7	−32.2
TS	−39.6	−38.6	−26.1
Methylenecyclopropene	−76.7	−74.3	−61.2

Notes: [a]Absolute energies in Hartree, energy differences ΔE, enthalpy differences $\Delta H(298)$, and free energy differences $\Delta G(298)$ in kcal mol^{-1}. Relative energies (enthalpies) of TS and product are given with respect to the reactants. For iodine (reaction 4d), the SDD pseudopotentials [57] were applied.

reaction between this carbene and difluoroacetylene. They found unexpectedly perfluoro allenyl carbene, which after irradiation led to the corresponding MCP. These observations verify that electronic and environmental factors can convert a hidden intermediate into a real one.

4.4. *Mechanistic results*

On the basis of the mechanistic analysis carried out in this work for reaction (1), three sub-reactions can be defined: biradical formation, biradical-carbene rearrangement, carbene-cyclization (Scheme 1). Only the latter is a pericyclic reaction, to which the Woodward–Hoffmann rules can be applied. This however is problematic because the carbene-cyclization involves rotation of an excocyclic methylene group and a flipping of a CH bond from *cis* to *trans* position, which are not pericyclic processes and exclude a state or orbital analysis based on symmetry. On the background of this work, the application of the Woodward–Hoffmann rules to reaction (1) as a chelotropic non-linear symmetry-allowed reaction is questionable. The existence of a low barrier is a result of a favourable charge-transfer situation rather than orbital symmetry. In the same way, orbital symmetry cannot help to predict the changes caused by fluorination. Of course, one has also to consider that the Woodward–Hoffmann rules can only be applied to pericyclic concerted reactions. Since reaction (2) represents a two-step reaction with intermediate, and the RC of the allenyl carbene rearrangement to **MCP** does not possess any symmetry, one might argue that use of the orbital symmetry rules is not justified anyway.

Based on the URVA analysis of the mechanism of reaction (1), one can predict the mechanism of reaction (2), especially the change from a concerted to a non-concerted reaction. Similarly, one can predict mechanistic changes when replacing H atoms by halogens, electropositive atoms, bulky functional groups, conjugated systems, etc. For example, chlorination will lead to an allenylcarbene intermediate structure that is no longer stable and bromation or iodation will have a similar effects on the mechanism of reaction (1). These predictions are based on the fact that the pseudo-π orbital of X_2C in $X_2C{=}C$: will more strongly donate to the empty in-plane pπ orbital at

C3 (Scheme 3c), which is confirmed by the calculated populations of the latter orbital (Br: 186; I: 280 melectron, Scheme 3d).

Larger parts of the mechanistic analysis of reaction (1) presented in this work are based on DFT calculations. As noted before, CASSCF and CASPT2 calculations confirm the DFT mechanism and energetics. This however depends on the active space chosen. With the (8,8) space a biradical intermediate corresponding to 1,3-butadienediyl biradical was found at the CASSCF level due to the fact that the active space chosen exaggerates the stability of this biradical. The combined URVA analyses of reaction 2 and the reaction leading from the biradical intermediate to the final product reveals a slightly changed reaction mechanism, in which the singlet excited state of allenyl carbene is missing. This is a consequence of the fact that the (8,8) CASSCF description of the allenyl carbene is insufficient. Increasing the active space from (8,8) to (10,9) and finally to (12,9) at the CASSCF/6-311G(d,p) level of theory leads to the vanishing of the biradical intermediate and the occurrence of two hidden intermediates in the form of 1,3-butadienediyl biradical and allenyl carbene, i.e. the DFT/B3LYP reaction mechanism is reestablished. The same is true at the CASPT2(8,8) and CASPT2(12,11) or RASPT2(12,11) levels of theory. The inclusion of second order perturbation theory at the CASSCF level also confirms the energetics of the reaction: reaction (1) is predicted to proceed via a small barrier of just $2\,\mathrm{kcal\,mol^{-1}}$ with a reaction energy of $-63\,\mathrm{kcal\,mol^{-1}}$. CASSCF results differ from these values considerably because of the lack of dynamical electron correlation.

It is a common belief that the energetics of a chemical reaction is best suited for the analysis of its mechanism. Terms such as reaction concertedness, reaction intermediates, etc. are based on energy criteria. There have been attempts to use the energy changes along the reaction path to determine a reaction force and to partition the reaction path into zones according to properties of the reaction force [62,63]. These attempts can be very useful to understand the reaction mechanism, however they do not reveal the sequence of chemical processes as provided by the reaction path curvature and the phases derived therefrom. This is a consequence of the fact that the energy is an accumulative descriptor of all changes taking place along the reaction path that hides details of the chemical processes [17]. Nevertheless, a complementary analysis of reaction force and reaction path curvature can lead to a better understanding of the reaction mechanism.

Although the energetics of a reaction determines reaction rate and product stability, the reaction mechanism is better understood when analysing the major structural changes of the RC as reflected in the RP curvature [15–17]. This way of analysing reaction mechanism leads to much more detail and makes it possible to recognize (dis)similarities between different reaction types and provides a better basis to predict and by this to control changes in the reaction mechanism. The RP curvature is the basis of the concept of hidden intermediates and hidden transition states. These structures occupy transient positions on the PES along the RP, which contrary to the stationary points of a reaction have not any direct chemical meaning. However, as points with distinct structures they make it possible to characterize the rearrangements of the RC, which leads in result to a detailed analysis of the reaction mechanism.

Chemists have always tried to reduce the huge manifold of different chemical reactions to a limited number of prototypical reactions such as substitutions, eliminations, additions, cycloadditions, etc. The research pursued in this and previous papers is aimed at further reducing the number of prototypical reaction steps by identifying the different phases of chemical reactions and then using these reaction phases to find similarities between seemingly different reaction types. In this way, a new understanding of chemical reactions is obtained thus leading to an efficient strategy for controlling them.

Acknowledgement

EK and DC thank the National Science Foundation (Grant CHE 071893) and Southern Methodist University, Dallas for supporting this work.

References

[1] F.O. Rice and E. Teller, J. Chem. Phys. **6**, 489 (1938); *ibid*. **7**, 199 (1939).
[2] J. Franck and E. Rabinowitch, Z. Elektrochem. **36**, 794 (1930).
[3] J. Hine, J. Org. Chem. **31**, 1236 (1966).
[4] O.S. Tee, J. Am. Chem. Soc. **91**, 7144 (1969); O.S. Tee and K. Yates, *ibid*. **94**, 3074 (1972).
[5] O.S. Tee, J.A. Altmann and K. Yates, J. Am. Chem. Soc. **96**, 3141 (1974).
[6] R.B. Woodward and R. Homann, Angew. Chem. Int. Ed. Engl **8**, 781 (1969); R.B. Woodward, and R. Hoffmann, *The Conservation of Orbital Symmetry* (Verlag Chemie, Weinheim, 1970).
[7] J. March, *Advanced Organic Chemistry, Reactions, Mechanisms, and Structure*, 3rd ed. (Wiley, New York, 1985).

[8] A.J. Stone, *International Series of Monographs on Chemistry 32 – The Theory of Intermolecular Forces* (Clarendon Press, Oxford, 1966); in *Molecular Interactions, from van der Waals to Strongly Bound Complexes*, edited by S. Scheiner (Wiley, New York, 1994); *Van der Waals Molecules II*, Chemical Reviews, **94**, 1 (1994); *Van der Waals Molecules III*, Chem. Rev. **100**, 1 (2000).

[9] M.J.S. Dewar and R.C. Dougherty, *The PMO Theory of Organic Chemistry* (McGraw-Hill, Plenum, New York, 1975).

[10] M.G. Evans, and E. Warhust, Trans. Faraday Soc. **34**, 614 (1938); H. Zimmerman, Acc. Chem. Res. **4**, 272 (1971); M.J.S Dewar, Angew. Chem. **83**, 859 (1971).

[11] J.C. Polanyi, Acc. Chem. Res. **5**, 161 (1972) and references therein; Science **236**, 680 (1987).

[12] W. Quapp, E. Kraka and D. Cremer, J. Phys. Chem. A **111**, 11287 (2007).

[13] H. Joo, E. Kraka, W. Quapp and D. Cremer, Mol. Phys. **105**, 2697 (2007).

[14] E. Kraka, in *Encyclopedia of Computational Chemistry*, edited by P.v.R. Schleyer, N.L. Allinger, T. Clark, J. Gasteiger, P.A. Kollman, H.F. Schaefer III, and P.R. Schreiner (Wiley, Chichester, 1998), Vol. 4, p. 2437.

[15] E. Kraka, in *Interdisciplinary Reviews – Computational Molecular Science, WIREs CMS*, edited by P.R. Schreiner and W. Allen (Wiley, Chichester, 2011), submitted.

[16] E. Kraka and D. Cremer, Acc. Chem. Res. **43**, 591 (2010).

[17] D. Cremer and E. Kraka, Curr. Org. Chem. (2010) in press.

[18] Z. Konkoli, E. Kraka and D. Cremer, J. Phys. Chem. A **101**, 1742 (1997).

[19] Z. Konkoli, D. Cremer and E. Kraka, J. Comput. Chem. **18**, 1282 (1997).

[20] D. Cremer, A. Wu and E. Kraka, Phys. Chem. Chem. Phys. **3**, 674 (2001).

[21] E. Kraka, A. Wu and D. Cremer, J. Phys. Chem. A **107**, 9008 (2003).

[22] E. Kraka and D. Cremer, J. Phys. Org. Chem. **15**, 431 (2002).

[23] W.H. Miller, N.C. Handy and J.E. Adams, J. Phys. Chem. A **72**, 99 (1980).

[24] K. Fukui, J. Phys. Chem. **74** 4161 (1970); Acc. Chem. Res. **14**, 363 (1981).

[25] Z. Konkoli and D. Cremer, Int. J. Quantum Chem. **67**, 1 (1998); Z. Konkoli, L.A. Larsson, and D. Cremer, Int. J. Quantum Chem. **67**, 11 (1998); Int. J. Quantum Chem. **67**, 291 (1998).

[26] D. Cremer, J.A. Larsson, and E. Kraka, in *Theoretical and Computational Chemistry, Vol. 5, Theoretical Organic Chemistry*, edited by C. Párkányi (Elsevier, Amsterdam, 1998), p. 259.

[27] E. Kraka, J.A. Larsson and D. Cremer, in *Generalization of the Badger Rule Based on the Use of Adiabatic Vibrational Modes in Computational IR Spectroscopy*, edited by J. Grunenberg (Wiley, New York, 2010), in press.

[28] D. Cremer and E. Kraka, Angew. Chem. **96**, 612 (1984); Int. Edt. Engl. 23, **627** (1984); Croatica Chem. Acta **57**, 12591 (1984).

[29] E. Kraka and D. Cremer, in *Theoretical Models of Chemical Bonding. The Concept of the Chemical Bond*, edited by Z.B. Maksic (Springer Verlag, Heidelberg, 1990), Vol. 2, p. 453.

[30] R.F.W. Bader, *Atoms in Molecules, a Quantum Theory*, in *International Series Monographs on Chemistry 22* (Clarendon Press, Oxford, 1995).

[31] P. Hohenberg, and W. Kohn, Phys. Rev. **136**, B864 (1994); W. Kohn, and L. Sham, J. Phys. Rev. **140**, A1133 (1965); see also R.G. Parr and W. Yang, *International Series of Monographs on Chemistry 16: Density-Functional Theory of Atoms and Molecules* (Oxford University Press, New York, 1989).

[32] K. Raghavachari, G.W. Trucks, J.A. Pople and M. Head-Gordon, Chem. Phys. Lett. **157**, 479 (1989).

[33] K. Wolinski, H.L. Sellers and P. Pulay, Chem. Phys. Lett. **140**, 225 (1987); K. Wolinski and P. Pulay, J. Chem. Phys. **90**, 3647 (1989); K. Wolinski, Theor. Chim. Acta **82**, 459 (1992); Z. Konkoli, Ph.D. thesis, Göteborg, Sweden, 1996.

[34] A.M. Mebel, K. Morokuma and M.C. Lin, J. Chem. Phys. **103**, 7414 (1995); for the G-methods as such, see L.A. Curtiss, K. Raghavachari, P.C. Redfern, V. Rassolov, and J.A. Pople, J. Chem. Phys. **109**, 7764 (1998).

[35] R. Bauernschmitt and R. Ahlrichs, J. Chem. Phys. **104**, 9047 (1996).

[36] J. Graëenstein, E. Kraka and D. Cremer, Chem. Phys. Lett. **288**, 593 (1998).

[37] A.D. Becke, Phys. Rev. **A38**, 3098 (1988).

[38] C. Lee, W. Yang and R.G. Parr, Phys. Rev. **B37**, 785 (1988).

[39] A.D. Becke, J. Chem. Phys. **98**, 5648 (1993); see also J.P. Stevens, F.J. Devlin, C.F. Chablowski, and M.J. Frisch, J. Phys. Chem. **98**, 11623 (1994).

[40] CASSCF: B. Roos, in *Ab initio Methods in Quantum Chemistry, Vol. II*, edited by K.P. Lawley, In series *Advances in Chemical Physics*, Vol. 69 (Wiley, Chichester, 1987), p. 399.

[41] P.C. Hariharan and J.A. Pople, Theoret. Chim. Acta **28**, 213 (1973).

[42] R. Krishnan, M. Frisch and J.A. Pople, J. Chem. Phys. **72**, 4244 (1980).

[43] T. Dunning Jr, J. Chem. Phys. **99**, 1007 (1989).

[44] A.D. Becke, J. Chem. Phys. **88**, 2547 (1988).

[45] F. Boys and F. Bernardi, Mol. Phys. **19**, 553 (1970).

[46] A.E. Reed, L.A. Curtiss and E. Weinhold, Chem. Rev. **88**, 899 (1988).

[47] T. Carrington Jr and W.H. Miller, J. Chem. Phys. **84**, 3942 (1986).

[48] M. Page and J.W. McIver Jr, J. Chem. Phys. **88**, 922 (1988).
[49] W. Quapp, Theor. Chim. Acta **75**, 447 (1989).
[50] S. Kato and K. Morokuma, J. Chem. Phys. **73**, 3900 (1980).
[51] E. Kraka, J. Gräfenstein, M. Filatov, A. Wu, H. Joo, D. Izotov, J. Gauss, Y. He, Z. He, V. Polo, F. Reichel, Z. Konkoli, L. Olsson, and D. Cremer, *COLOGNE 2010* (Southern Methodist University, Dallas, 2010).
[52] M.W. Schmidt, K.K. Baldridge, J.A. Boatz, S.T. Elber, M.S. Gordon, J.J. Jensen, S. Koseki, N. Matsunaga, K.A. Nguyei, S. Su, T.L. Windus, M. Dupuis and J.A. Montgomery, J. Comput. Chem. **14**, 1347 (1993).
[53] M.J. Frisch, G.W. Trucks, H.B. Schlegel, G.E. Scuseria, M.A. Robb, J.R. Cheeseman, J.A. Montgomery Jr, T. Vreven, K.N. Kudin, J.C. Burant, J.M. Millam, S.S. Iyengar, J. Tomasi, V. Barone, B. Mennucci, M. Cossi, G. Scalmani, N. Rega, G.A. Petersson, H. Nakatsuji, M. Hada, M. Ehara, K. Toyota, R. Fukuda, J. Hasegawa, M. Ishida, T. Nakajima, Y. Honda, O. Kitao, H. Nakai, M. Klene, X. Li, J.E. Knox, H.P. Hratchian, J.B. Cross, V. Bakken, C. Adamo, J. Jaramillo, R. Gomperts, R.E. Stratmann, O. Yazyev, A.J. Austin, R. Cammi, C. Pomelli, J.W. Ochterski, P.Y. Ayala, K. Morokuma, G.A. Voth, P. Salvador, J.J. Dannenberg, V.G. Zakrzewski, S. Dapprich, A.D. Daniels, M.C. Strain, O. Farkas, D.K. Malick, A.D. Rabuck, K. Raghavachari, J.B. Foresman, J.V. Ortiz, Q. Cui, A.G. Baboul, S. Clifford, J. Cioslowski, B.B. Stefanov, G. Liu, A. Liashenko, P. Piskorz, I. Komaromi, R.L. Martin, D.J. Fox, T. Keith, M.A. Al-Laham, C.Y. Peng, A. Nanayakkara, M. Challacombe, P.M.W. Gill, B. Johnson, W. Chen, M.W. Wong, C. Gonzalez and J.A. Pople, *Gaussian 03, Revision C.02* (Gaussian, Inc., Wallingford, CT, 2004).
[54] CFOUR, a quantum chemical program package written by J.F. Stanton, J. Gauss, M.E. Harding, P.G. Szalay, with contributions from A.A. Auer, R.J. Bartlett, U. Benedikt, C. Berger, D.E. Bernholdt, Y.J. Bomble, O. Christiansen, M. Heckert, O. Heun, C. Huber, T.-C. Jagau, D. Jonsson, J. Juselius, K. Klein, W.J. Lauderdale, D.A. Matthews, T. Metzroth, D.P. O'Neill, D.R. Price, E. Prochnow, K. Ruud, F. Schiffmann, S. Stopkowicz, A. Tajti, J. Vazquez, F. Wang, J.D. Watts and the integral packages MOLECULE (J. Almlöf and P.R. Taylor), PROPS (P.R. Taylor), ABACUS (T. Helgaker, H.J.Aa. Jensen, P. Jorgensen, and J. Olsen), and ECP routines by A.V. Mitin and C. van Wöllen.
[55] D. Cremer, E. Kraka, H. Joo, J.A. Stearns and T.S. Zwier, Phys. Chem. Chem. Phys. **8**, 5304 (2006).
[56] A.M. Mebel, V.V. Kislov and R.I. Kaiser, J. Chem. Phys. **125**, 133113 (2006).
[57] M. Dolg, U. Wedig, H. Stoll and H. Preuss, J. Chem. Phys. **86**, 866 (1987).
[58] G.A. Natanson, B.C. Garrett, T.N. Truong, T. Joseph and D.G. Truhlar, J. Chem. Phys. **94**, 7875 (1991).
[59] Y.-Y. Chuang and G.D. Truhlar, J. Phys. Chem. A **102**, 242 (1998).
[60] D. Lloyd, *Studies in Organic Chemistry 16 – Non-Benzoid Conjugated Carbocyclic Compounds* (Elsevier, New York, 1984).
[61] C. Kötting, W. Sander and M. Senzlober, Chem. Eur. J. **4**, 2360 (1998).
[62] A. Toro-Labbe, S. Gutierrez-Oliva, J.S. Murray and P. Politzer, Mol. Phys. **105**, 2619 (2007).
[63] A. Toro-Labbe, S. Gutierrez-Oliva, P. Politzer, and J.S. Murray, in *Theory of Chemical Reactivity*, edited by P. Chattaraj (Taylor and Francis, Boca Raton, 2008), Chapter 21.